Characterization of Ross River Virus Tropism and Virus-Induced Inflammation in a Mouse Model of Viral Arthritis and Myositis

Thomas E. Morrison,[1,2,3] Alan C. Whitmore,[3] Reed S. Shabman,[1,2,3] Brett A. Lidbury,[4] Suresh Mahalingam,[4] and Mark T. Heise[1,2,3]*

Department of Genetics,[1] Department of Microbiology and Immunology,[2] and Carolina Vaccine Institute,[3] University of North Carolina at Chapel Hill, Chapel Hill, North Carolina 27599, and Viral Arthritis/Asthma Research Group, School of Health Sciences, University of Canberra, Canberra, ACT 2601, Australia[4]

Mosquito-borne alphaviruses are a significant cause of both encephalitic and arthritic disease in humans worldwide. In contrast to the encephalitic alphaviruses, the pathogenesis of alphavirus-induced arthritic disease is not well understood. Utilizing a mouse model of Ross River virus (RRV) disease, we found that the primary targets of RRV infection are bone, joint, and skeletal muscle tissues of the hind limbs in both outbred CD-1 mice and adult C57BL/6J mice. Moreover, histological analyses demonstrated that RRV infection resulted in severe inflammation of these tissues. Characterization of the inflammatory infiltrate within the skeletal muscle tissue identified inflammatory macrophages, NK cells, and CD4$^+$ and CD8$^+$ T lymphocytes. To determine the contribution of the adaptive immune system, the outcome of RRV-induced disease was examined in C57BL/6J RAG-1$^{-/-}$ mice, which lack functional T and B lymphocytes. RAG-1$^{-/-}$ and wild-type mice developed similar disease signs, infiltration of inflammatory macrophages and NK cells, and muscle pathology, suggesting that the adaptive immune response does not play a critical role in the development of disease. These results establish the mouse model of RRV disease as a useful system for the identification of viral and host factors that contribute to alphavirus-induced arthritis and myositis.

Mosquito-borne arthritogenic alphaviruses, such as Ross River virus (RRV), Chikungunya virus, O'nyong-nyong virus, and Mayaro virus, are a significant cause of infectious rheumatic disease worldwide (10, 36). For example, RRV, which is endemic to Australia, causes several thousand cases of infectious polyarthritis per year. Furthermore, these viruses are a major concern due to their ability to emerge and cause major epidemics. This is illustrated by an epidemic of Ross River virus disease in the South Pacific which involved greater than 60,000 patients in 1979 to 1980 (13) and a 1959 to 1962 epidemic of O'nyong-nyong fever in Africa which involved at least 2 million patients (39). This is further reinforced by the reports that RRV has reemerged in Fiji, where the virus had apparently been absent since the 1979–1980 epidemic (19), and by recent Chikungunya and O'nyong-nyong fever outbreaks in Africa and Asia (18, 21, 27, 30).

Severe arthritis/arthralgia is a shared symptom of many of the alphavirus-induced diseases. The clinical course of RRV infection, which causes severe acute polyarthritis, is one of the best-characterized alphavirus-induced arthritic diseases. RRV-induced disease symptoms include fever, rash, myalgia, and pain and stiffness in the joints (13). Muscle and joint pain in afflicted individuals may persist for weeks to months, and anti-inflammatory drugs are the best current treatment for RRV disease (12, 13). The arthritic disease is thought to be initiated by viral replication and inflammatory infiltrates in the affected joints (7, 35). This is largely based on the detection of RRV

RNA in the synovia from the knees of patients infected with RRV (35) and the detection of RRV antigen in synovial infiltrates from affected joints (6). RRV-induced arthritis is characterized by inflammatory infiltrates comprised largely of mononuclear cells. Characterization of these infiltrates suggests that monocytes/macrophages are a major constituent of the infiltrate (6, 14), while immunohistological studies of synovial biopsy samples have also identified CD4$^+$ and CD8$^+$ T lymphocytes within the inflammatory infiltrates (35).

Although a large number of studies have focused on the pathogenesis of alphavirus-induced encephalitis, the mechanisms by which arthritogenic alphaviruses cause disease are largely unknown. Recently, Lidbury et al. reported that RRV-infected 17- to 21-day-old outbred mice developed severe disease characterized by inflammation of muscle tissue and muscle damage (22). That study demonstrated that disease signs, such as hind limb dragging and muscle pathology, were ameliorated following treatment of mice with macrophage-toxic agents, suggesting a critical role for host immunity and macrophages in mediating RRV-induced disease.

In this study, we utilized the mouse model of RRV disease described by Lidbury et al. (22) to identify the primary sites of RRV replication. In addition, we report that RRV-infected 24-day-old C57BL/6J (B6) mice developed severe disease characterized by inflammation of hind limb bone and joint-associated tissues as well as skeletal muscle tissue. Finally, to determine the contribution of adaptive immune responses to the development of RRV disease, we examined the outcome of RRV infection in C57BL/6J RAG-1$^{-/-}$ mice, which lack functional T and B lymphocytes. In addition to elucidating mechanisms by which arthritogenic alphaviruses cause disease, these findings indicate that RRV infection of B6 mice represents a

* Corresponding author. Mailing address: The Carolina Vaccine Institute, University of North Carolina at Chapel Hill, 827 Mary Ellen Jones Bldg., CB no. 7292, Chapel Hill, NC 27599. Phone: (919) 843-1492. Fax: (919) 843-6924. E-mail: heisem@med.unc.edu.

powerful animal model for studying virus-induced inflammation and immunopathology.

MATERIALS AND METHODS

Viruses and cells. Viral stocks of the wild-type T48 strain of RRV were generated by in vitro transcription of SacI-linearized plasmid pRR64 (generously provided by Richard Kuhn, Purdue University), which encodes the full-length T48 cDNA clone (20), by using SP6-specific mMessage mMachine in vitro transcription kits (Ambion). The T48 stain of RRV was initially isolated from *Aedes vigilax* mosquitoes in Queensland, Australia (5). Prior to cDNA cloning, the virus was passaged 10 times in suckling mouse brain, followed by two passages on Vero cells (3). Full-length transcripts were electroporated into BHK-21 cells (ATCC CRL 8544) using a Bio-Rad electroporator as described previously (16). Culture supernatants were harvested at 24 h after electroporation, centrifuged for 20 min at 3,000 rpm, aliquoted, and stored at −80°C. Virus was titrated by plaque assay on BHK-21 cells as described previously (34).

To generate an RRV that expresses the enhanced green fluorescent protein (EGFP), a second RRV 26S promoter sequence was inserted at the 3′ end of the viral genome, followed by the coding sequence for EGFP. In brief, the 26S subgenomic promoter region of Ross River virus from nucleotides 7300 to 7507 of pRR64 was PCR amplified. The resulting PCR product had engineered sequential NotI and SpeI restriction sites 46 nucleotides downstream of the 26S RNA start site and was flanked by HindIII sites. This PCR product was introduced into position 11,330 in the pRR64 sequence to produce the plasmid pRR64(26S). The EGFP coding sequence was removed from plasmid pREP91Egfp (16) and introduced into pRR64(26S) using the NotI and SpeI restriction sites downstream of the second 26S subgenomic promoter to generate plasmid pRR64-Egfp. pRR64-Egfp was linearized with SacI and used as a template for in vitro transcription and virus production as described above for pRR64. EGFP expression in virus-infected cells was confirmed by fluorescence microscopy.

BHK-21 cells were grown in α-minimal essential medium (Gibco) supplemented with 10% donor calf serum, 10% tryptose phosphate broth, and 0.29 mg/ml L-glutamine.

Mice. Specific-pathogen-free pregnant female outbred CD-1 mice at 13 to 15 days of gestation were obtained from Charles River Breeding Laboratories (Raleigh, North Carolina). C57BL/6J mice, C57BL/6J RAG-1$^{-/-}$ mice, and μMT mice were obtained from The Jackson Laboratory (Bar Harbor, Maine) and bred in-house. μMT mice carry a stop codon and the neomycin gene cassette in the first transmembrane exon of the μ chain, resulting in B-lymphocyte deficiency (17). In some experiments, mice were obtained from the animal breeding establishment in the John Curtin School of Medical Research, Australia. Animal housing and care at UNC were in accordance with all UNC-CH Institutional Animal Care and Use Committee guidelines. Although RRV is classified as a biosafety level 2 pathogen, due to its exotic nature, all mouse studies in the United States were performed in a biosafety level 3 laboratory.

Mice were inoculated in the left rear footpad with 10^3 PFU of virus in diluent (phosphate-buffered saline [PBS]–1% donor calf serum) in a 10-μl volume. Alternatively, in a subset of studies, mice received the virus subcutaneously in the thorax below the right forelimb in a 50-μl volume. No significant differences in viral replication or development of disease were detected in mice inoculated from either route. Mock-infected animals received diluent alone. Mice were monitored for disease signs and weighed at 24 h intervals. The clinical signs of disease were determined by assessing grip strength and altered gait. Grip strength and hind limb weakness were assessed by testing the ability of each mouse to support itself while suspended from a wire cage. Mice were scored as follows: 0, no disease signs; 1, ruffled fur; 2, very mild hind limb weakness; 3, mild hind limb weakness; 4, moderate hind limb weakness and dragging of hind limbs; 5, severe hind limb weakness/dragging; 6, complete loss of hind limb function; 7, moribund; and 8, death. To determine viral titers in tissues, mice were sacrificed by exsanguination and perfused with 1× PBS. The popliteal lymph node, right and left ankles, right and left quadriceps muscles, spleen, brain, and spinal cord (divided into thoracic and lumbar regions) were removed by dissection and weighed. Tissues were homogenized in 1× PBS supplemented with 1% donor calf serum, Ca^{2+}, and Mg^{2+} and stored at −80°C until viral load was assessed by a standard plaque assay on BHK-21 cells.

For histological analysis, mice were sacrificed by exsanguinations and perfused with PBS–4% paraformaldehyde, pH 7.3. Following fixation of tissues and further decalcification of bone-associated tissues, all tissues were embedded in paraffin and 5-μm sections were prepared by the UNC histopathology core facility. To determine the extent of inflammation, tissues were stained with hematoxylin and eosin (H & E). Myelin was stained with luxol fast blue followed
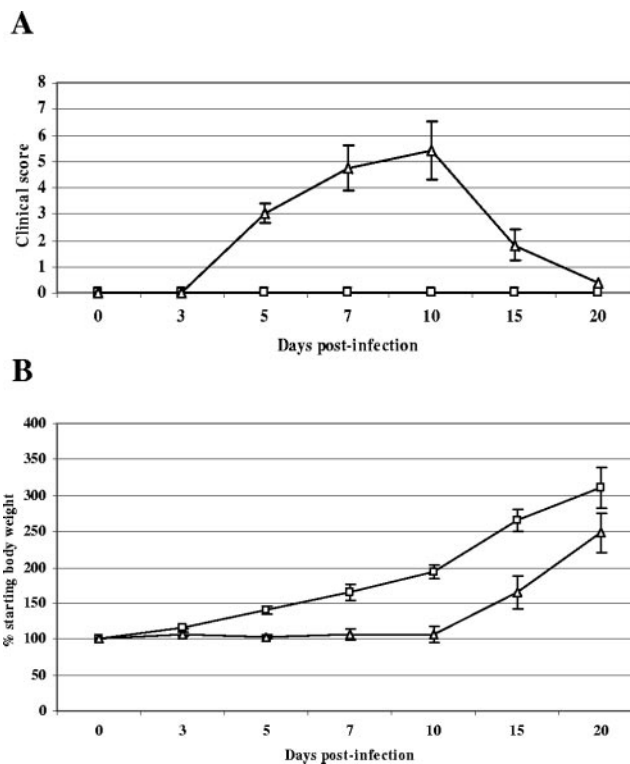

FIG. 1. Ross River virus-induced disease in 15-day-old CD-1 mice. Fifteen-day-old CD-1 mice were infected with 10^3 PFU of RRV (Δ) by subcutaneous injection in the left rear footpad. Mock-infected mice (□) were injected with diluent alone. (A) Mice were scored for development of hind limb dysfunction and disease based on the following scale: 0, no disease signs; 1, ruffled fur; 2, very mild hind limb weakness; 3, mild hind limb weakness; 4, moderate hind limb weakness and dragging of hind limbs; 5, severe hind limb weakness/dragging; 6, complete loss of hind limb function; 7, moribund; and 8, death. (B) Mice were monitored for weight gain or loss at 24-h intervals. Each data point represents the arithmetic mean ± standard deviation (SD) for 7 (mock-infected) or 25 (RRV-infected) mice.

by a periodic acid-Schiff counterstain. Sections were analyzed using a Nikon Microphot-FXA microscope fitted with an Optronics DEI 750 three-chip charge-coupled-device camera for digital imaging.

In situ hybridization. In situ hybridization was performed as described previously (15). Briefly, a ^{35}S-labeled RRV-specific riboprobe (complementary for RRV nucleotides 7300 to 7775) was generated with an SP6-specific MAXIscript in vitro transcription kit (Ambion) from a NotI-linearized plasmid. A riboprobe complementary for the EBER2 gene from Epstein-Barr virus was used as a negative control. Deparaffinized tissue sections were hybridized with 5 × 10^4 cpm/μl of ^{35}S-labeled riboprobes overnight. Tissues were washed, dehydrated through graded ethanol, and immersed in Nitro Blue Tetrazolium autoradiography emulsion (Kodak). Following development, sections were counterstained with hematoxylin and silver grain deposition was analyzed by light microscopy.

Flow cytometry. Mice were inoculated as described above, sacrificed by exsanguination at 5 and 7 days postinfection (dpi), and perfused for 10 min with 1× PBS. Quadriceps muscles and spleens were dissected, minced, and incubated for 2 h with vigorous shaking at 37°C in digestion buffer (RPMI 1640, 10% fetal bovine serum, 15 mM HEPES, 2.5 mg/ml collagenase A [Roche], 1.7 mg/ml DNase I [Sigma]). Following digestion, cells were passed through a 40-μm cell strainer, red blood cells were lysed (spleens only), cells were washed in wash buffer (1× Hanks balanced salt solution, 15 mM HEPES), and total viable cells were determined by trypan blue exclusion. Cells were incubated with anti-mouse FcγRII/III (2.4G2; BD Pharmingen) for 20 min on ice to block nonspecific antibody binding and then stained in fluorescence-activated cell sorting staining buffer (1× Hanks balanced salt solution, 1% fetal bovine serum, 2% normal rabbit serum) with the following antibodies from eBioscience: F4/80-fluorescein
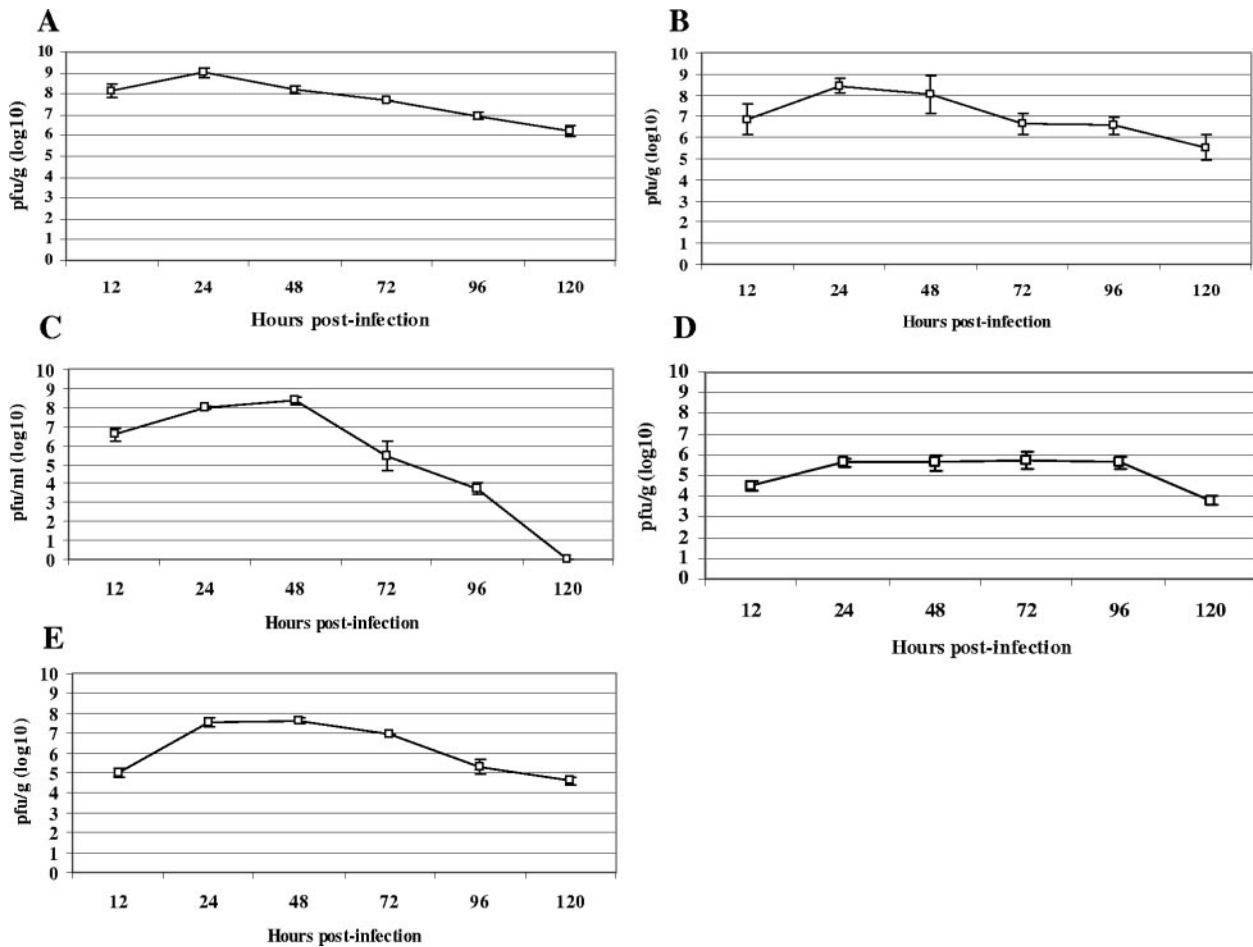
FIG. 2. Ross River virus tissue titers in 15-day-old CD-1 mice. Fifteen-day-old CD-1 mice were infected with 10^3 PFU of RRV by subcutaneous injection in the left rear footpad. At 12, 24, 48, 72, 96, and 120 hpi, ankle (A), quadriceps muscle (B), serum (C), brain (D), and spleen (E) were harvested and homogenized, and the amount of infectious virus present was quantified by plaque assay on BHK-21 cells. Each data point represents the arithmetic mean $\pm$ SD for three mice.

isothiocyanate, NK1.1-phycoerythrin, Ly6C/G (Gr1)-phycoerythrin, CD3-fluorescein isothiocyanate, CD4-biotin, CD19–allophycocyanin (APC), CD8α-APC, CD11b-APC, and B220-APC. Biotin conjugates were detected with streptavidin-peridinin chlorophyll protein (eBioscience). Cells were fixed overnight in 2% paraformaldehyde and analyzed on a FACSCalibur (Becton Dickinson) using CellQuest software.

RESULTS

Ross river virus replicates in bone and joint-associated tissues and skeletal muscle. Infection of 14- to 21-day-old outbred mice with the T48 strain of RRV has previously been demonstrated to induce inflammation and destruction of hind limb skeletal muscle (22). To further evaluate this model for its utility in investigating the pathogenesis of RRV-induced disease, we sought to identify the sites of viral replication in vivo. As a first step, studies were performed to ensure that CD-1 mice exhibited the same phenotype upon RRV infection as the Swiss outbred mice used in previous studies (22). Fourteen- to 15-day-old CD-1 outbred mice were inoculated with 10^3 PFU of RRV by subcutaneous injection in the left rear footpad and monitored for virus-induced morbidity and mortality. Infected mice developed severe disease signs characterized by loss of

hind limb gripping, hind limb dragging (Fig. 1A), and lack of weight gain (Fig. 1B). These disease signs became apparent 4 to 5 dpi, peaked at 10 dpi, and resolved by 20 dpi (Fig. 1A and B). These findings are consistent with previous observations of Swiss outbred mice. However, up to 75% of Swiss outbred mice were reported to have succumbed to infection (22), whereas only 16% of CD-1 outbred mice used in this study succumbed to infection.

To begin to identify the sites of RRV replication in vivo, viral replication in tissues at various times postinfection was assessed by plaque assay. Peak titers of infectious virus were detected at 24 to 48 h postinfection (hpi) (Fig. 2). Viral titers of up to 10^9 PFU/gram were detected in ankle-associated tissue (Fig. 2A) and quadriceps muscle tissue (Fig. 2B). In contrast, peak viral titers in the brain (Fig. 2D) and spleen (Fig. 2E) were markedly lower than those observed in both ankle and skeletal muscle tissues.

In order to identify specific sites of RRV replication, in situ hybridization using an ^{35}S-labeled riboprobe specific for RRV was performed on sections derived from hind limb tissues of 14- to 15-day-old CD-1 mice infected with RRV.
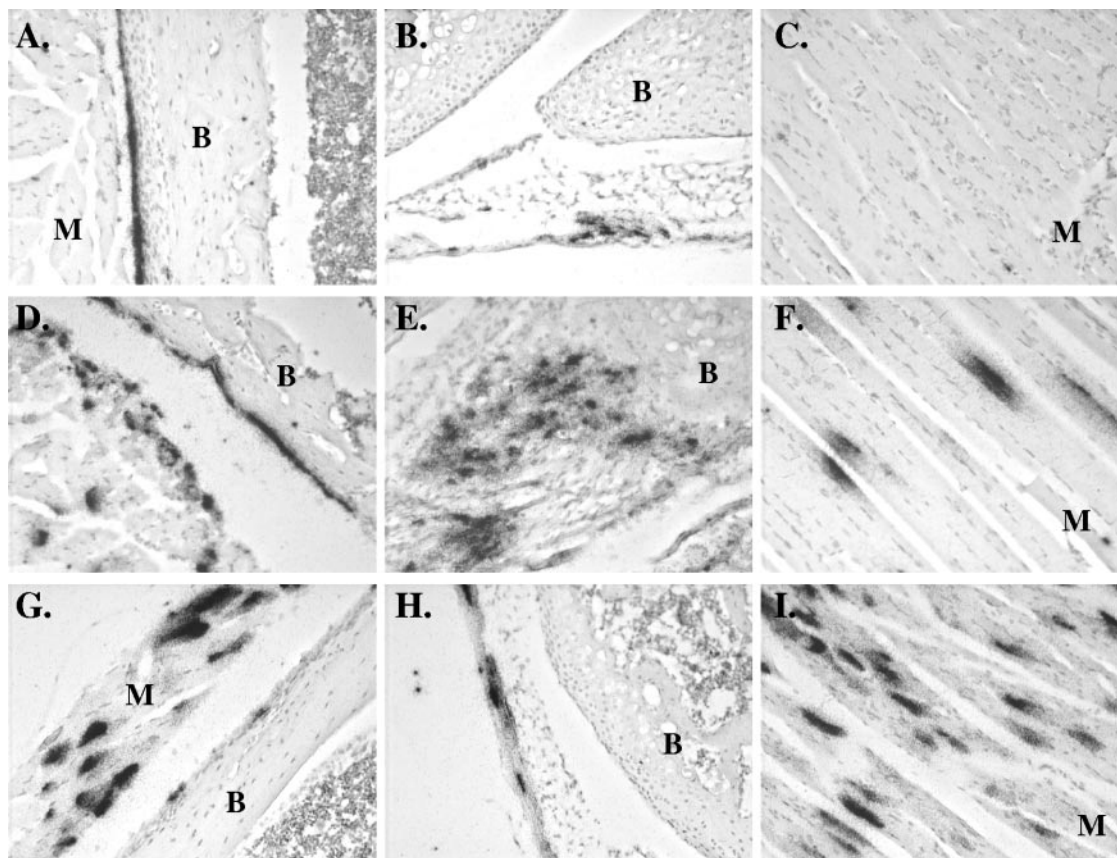
FIG. 3. Ross River virus replication within bone and joint-associated connective tissues and skeletal muscle tissue. Fifteen-day-old CD-1 mice were infected with 10^3 PFU of RRV by subcutaneous injection in the ventral thorax. Mock-infected mice were injected with diluent alone. Mice were sacrificed at 24 (A, B, C), 48 (D, E, F), and 72 (G, H, I) hours postinfection and perfused with 4% paraformaldehyde. Following decalcification, 5-μm-thick paraffin-embedded sections derived from the hind limbs were probed with ^{35}S-labeled riboprobes complementary for RRV (A-I) or the EBER2 gene from Epstein-Barr virus (data not shown). M, muscle; B, bone. (A) RRV-specific in situ signal in tarsal bone periosteum. (B) RRV-specific in situ signal in synovial connective tissue of the knee joint. (C) Absence of RRV-specific in situ signal in hind limb skeletal muscle. (D) RRV-specific in situ signal in tarsal bone periosteum and associated skeletal muscle. (E) RRV-specific in situ signal in synovial tissue of a tarsal joint. (F) RRV-specific in situ signal in hind limb skeletal muscle tissue. (G) RRV-specific in situ signal in metatarsal bone periosteum and associated skeletal muscle. (H) RRV-specific in situ signal in hind limb tendon. (I) RRV-specific in situ signal in hind limb skeletal muscle.

At 24 hpi, abundant RRV-specific signal was detected within cells of the periosteum lining bones of the hind limbs (Fig. 3A) and cells within synovial tissue of the knee joint (Fig. 3B). In addition, RRV-specific signal was observed in cells within tendons and ligaments and associated with articular surfaces (data not shown). A similar distribution of RRV replication within bone- and joint-associated tissues of the hind limbs was also detected at both 48 hpi (Fig. 3D and E) and 72 hpi (Fig. 3G and H). Interestingly, although RRV replication was not observed within myofibers of hind limb skeletal muscle tissue at 24 hpi (Fig. 3C), RRV-specific, in situ signal was detected within connective tissues, such as the perimysium and tendons, that are associated with skeletal muscle (data not shown). By 48 and 72 hpi, extensive signal was detected within the myofibers of skeletal muscle tissue (Fig. 3F and I). No signal was detected in tissue sections from infected animals hybridized with a riboprobe specific for the EBER2 gene from Epstein-Barr virus or in tissues from mock-infected animals hybridized with the RRV-specific riboprobe (data not shown).

To confirm the in situ hybridization studies, an RRV that expressed enhanced green fluorescent protein (RRV-EGFP) in infected cells was constructed by inserting the EGFP coding sequence downstream of a second 26S subgenomic promoter placed at the 3′ end of the viral genome (Fig. 4A). Initial studies demonstrated that RRV-EGFP was attenuated in 14- to 15-day-old CD-1 mice; however, infection of 10- to 12-day-old mice resulted in similar disease signs (data not shown). Therefore, 10- to 12-day-old CD-1 outbred mice were inoculated with 10^3 PFU of RRV-EGFP in the ventral thorax, mice were sacrificed at the times postinfection indicated in Fig. 4, and tissue sections were analyzed for GFP expression. At 24 to 48 hpi, extensive viral replication, as indicated by GFP expression, was observed in synovial tissues of hind limb joints. Major sites of replication included cells lining the synovial cavity of the ankle joint (Fig. 4A and B), cells within the persiosteum (Fig. 4C), and cells within the tendons at junctions with the skeletal muscle (data not shown). Though high viral titers were detectable by plaque assay within the skeletal muscle at 24 to 48 hpi (Fig. 2B), few GFP-positive cells were detectable in the
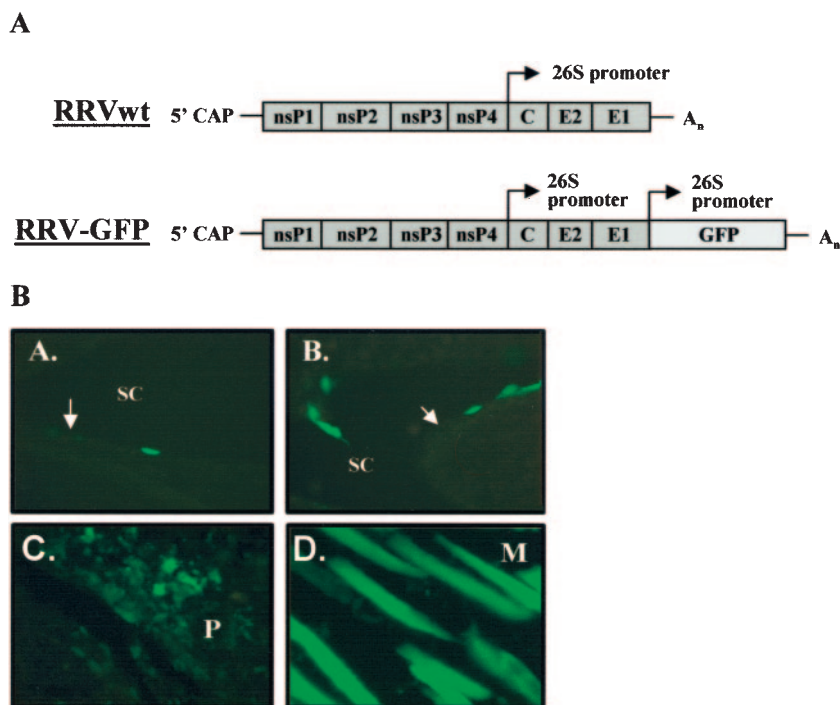
A

B

FIG. 4. Ross River virus double-promoter virus targets cells within joint, bone, and skeletal muscle tissues. (A) Schematic diagram of Ross River virus that was engineered to express EGFP by inserting a second RRV 26S subgenomic promoter at the 3′ end of the viral genome followed by the EGFP coding sequence. (B) Ten- to 12-day-old CD-1 mice were infected with 10^3 PFU of RRV-EGFP by subcutaneous injection in the ventral thorax. At 48 and 72 hpi, tissues were harvested and sections were analyzed for EGFP expression. SC, synovial cavity; M, muscle; P, periosteum. The white arrows indicate the articular surface. (Subpanel A) Synovial cavity in the foot at 48 hpi. (Subpanel B) Synovial cavity in the ankle at 48 hpi. (Subpanel C) Periosteum in the hind limb at 48 hpi. (Subpanel D) Hind limb skeletal muscle at 72 hpi.

skeletal muscle at these time points (data not shown). Consistent with the in situ hybridization studies, at 72 hpi, high levels of GFP expression were observed in large areas of hind limb skeletal muscle tissue (Fig. 4D). That GFP expression accurately represented the distribution of virally infected cells was confirmed by staining sections from RRV-GFP-infected mice with RRV-specific hyperimmune sera, which demonstrated that GFP-positive cells exhibited RRV-specific staining (data not shown).

Taken together, these data indicate that hind limb bone and joint-associated tissues and skeletal muscle tissue are primary targets for RRV infection. Furthermore, the in situ hybridization (Fig. 3) and GFP expression studies (Fig. 4) indicate that the initial viral titers in the skeletal muscle at 12 to 24 hpi may reflect either localized replication in connective tissue associated with skeletal muscle, such as the perimysium, or contamination of the muscle preparations with infected tendon that exhibited high levels of replication at early times. These findings also suggest that the virus may initially infect joint-associated connective tissues and subsequently spread into skeletal muscle tissue, although additional studies are required to truly address this possibility.

Ross river virus infection causes severe hind limb disease in C57BL/6J mice. Previous studies of mice have suggested that RRV infection induces an immunopathological inflammatory disease (22). To understand the components of the host immune response and other host determinants that contribute to RRV-induced disease, we sought to characterize the outcomes of RRV infection in inbred strains of mice as a starting point for studies of mice deficient for specific host factors. RRV infection of 15-day-old C57BL/6J (B6) mice resulted in severe hind limb dysfunction similar to that observed following infection of 15-day-old outbred CD-1 mice. However, disease became increasingly severe, and 100% of 15-day-old B6 mice succumbed to infection (Table 1). Therefore, older mice were evaluated for susceptibility to RRV disease. Infection of 24-day-old B6 mice resulted in severe morbidity similar to that observed in 14- to 15-day-old CD-1 mice (Fig. 5 and Table 1). Disease signs following RRV infection of 24-day-old B6 mice included failure to gain weight (Fig. 5B) and progressive symmetrical hind limb dysfunction ranging from loss of hind limb gripping ability to very severe hind limb dragging (Fig. 5A).

TABLE 1. Morbidity and mortality following RRV infection

Mice	Age (days)	Inoculum	No. of mice	% Morbidity	% Mortality	AST (days)[a]
CD-1	14–15	Mock	7	0	0	NA
		RRV	25	100	16	10 ± 0.8
C57BL/6	15	Mock	4	0	0	NA
		RRV	17	100	100	7 ± 0.7
C57BL/6	24	Mock	7	0	0	NA
		RRV	23	100	0	NA

[a] AST, average survival time; NA, not applicable.
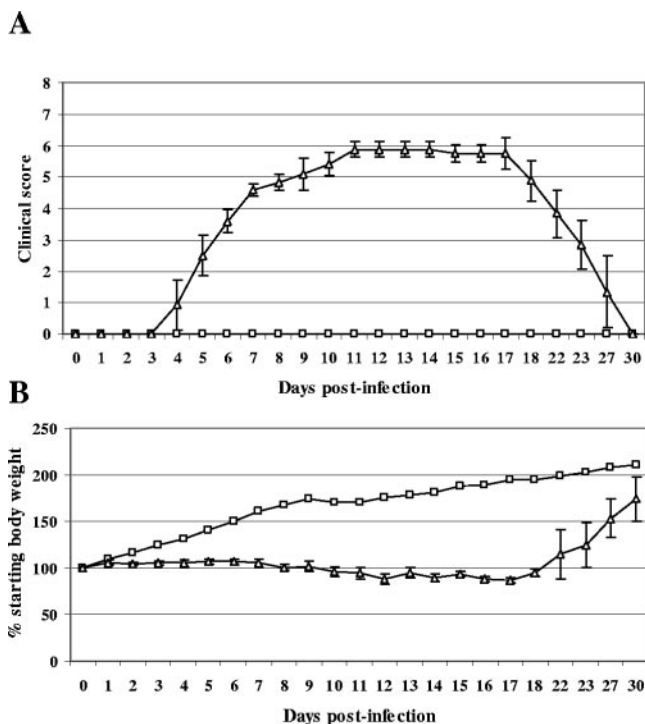
A

B

FIG. 5. Ross River virus infection induces severe hind limb disease in 24-day-old C57BL/6J mice. Twenty-four-day-old C57BL/6J mice were inoculated with 10^3 PFU of RRV (Δ) by subcutaneous injection in the left rear footpad. Mock-infected mice ($\square$) were injected with diluent alone. (A) Mice were scored for development of hind limb dysfunction and disease based on the following scale: 0, no disease signs; 1, ruffled fur; 2, very mild hind limb weakness; 3, mild hind limb weakness; 4, moderate hind limb weakness and dragging of hind limbs; 5, severe hind limb weakness/dragging; 6, complete loss of hind limb function; 7, moribund; and 8, death. (B) Mice were monitored for weight gain or loss at 24-h intervals. Each data point represents the arithmetic mean $\pm$ SD for three (mock-infected) or six (RRV-infected) animals. Data are representative of four independent experiments.

Disease signs, such as hunched posture, tremulousness, or spontaneous circling and falling, were not observed in RRV-infected mice. In addition, RRV-infected 24-day-old B6 mice appeared to completely recover from the disease by 25 to 30 dpi, as indicated by resumption of weight gain and an absence of observable disease signs (Fig. 5).

Ross river virus replicates in bone and joint-associated tissues and skeletal muscles of adult C57BL/6J mice. Plaque assays were performed to measure the amount of infectious virus within tissues of 24-day-old B6 mice at 12, 24, 48, 72, 96, and 120 hpi with RRV. Peak viral titers were detected at 24 to 48 hpi in all tissues examined (Fig. 6). Similar to findings for CD-1 mice, the highest viral titers detected were from ankle tissue, quadriceps muscle tissue, and serum (Fig. 6A, B, and C, respectively). In contrast, viral titers in the spleen (Fig. 6D), brain (Fig. 6E), and upper and lower spinal cord (Fig. 6F) were 10- to 1,000-fold lower on a PFU/gram basis. Consistent with the symmetrical signs of disease, viral titers detected in ankle and skeletal muscle tissue harvested from the injected limb and the contralateral limb (noninjected) were similar at each time

point (Fig. 6A and B), indicating that the observed replication pattern is not limited to the injected limb.

RRV infection induces inflammation of bone and joint-associated tissues and skeletal muscle of adult C57BL/6J mice. Comprehensive histological analyses of hind limb bone, joint, and skeletal muscle tissue, as well as tissues of the central nervous system, were performed to determine whether RRV infection of B6 mice resulted in inflammation and pathology at any of these sites. Little to no inflammation was observed at times earlier than 5 dpi. By 5 dpi, in contrast to what occurred with mock-infected mice (Fig. 7A), evaluation of bone and joints within the feet of RRV-infected mice revealed numerous inflammatory cells within the periosteum, synovial tissue, and associated skeletal muscle tissue (Fig. 7B). At 7 dpi, inflammation was absent in synovial tissue of mock-infected mice (Fig. 7C) but was again detected in synovial tissue of RRV-infected mice (Fig. 7D). Similarly, no inflammation was observed in quadriceps skeletal muscle tissue in mock-infected animals (Fig. 8A) or RRV-infected animals (Fig. 8B) at 3 dpi. The presence of inflammatory infiltrates was first observed in quadriceps muscle tissue at 5 dpi (Fig. 8C). Inflammation in skeletal muscle tissue reached peak severity by 7 and 10 dpi (Fig. 8D and E). Obvious signs of myofiber destruction, consistent with previous findings (22, 31), were observed at 7 and 10 dpi (Fig. 8D and E). Both the RRV-induced inflammation and pathology within hind limb tissues resolved by 25 to 30 dpi (Fig. 8F). This resolution included the presence of centralized nuclei within myofibers (Fig. 8F), indicating that muscle fiber regeneration was occurring within RRV-infected animals (2, 38). Unlike with hind limb bone, joint, and skeletal muscle tissues, we did not observe inflammatory infiltrates, demyelination, or other virus-induced pathology within brain and spinal cord tissues, including the spinal root (data not shown). Focal areas of hypercellularity and activated microglia were observed within the spinal cords of RRV-infected mice; however, these observations were quite subtle and were not associated with any overt pathology. Taken together, these findings indicate that the severe hind limb weakness and dysfunction that develops in B6 mice following RRV infection is most likely due to the severe inflammation and pathology observed in hind limb bone, joint, and skeletal muscle tissues.

Identification of inflammatory infiltrates in vivo. To begin to identify mechanisms involved in RRV-induced inflammation and pathology, the composition of inflammatory infiltrates within the hind limb skeletal muscle was analyzed by flow cytometry. The hind limb quadriceps muscle was chosen over joint tissues for these analyses due to the larger tissue volume resulting in greater cell yield. At 5 and 7 dpi, quadriceps muscle tissue from each of the hind limbs of mock-infected or RRV-infected mice were dissected, minced, and digested with collagenase A and DNase I to generate single-cell suspensions. To control for effects of the digestion protocol on cell surface antigen expression, splenocytes from mock-infected and RRV-infected animals were isolated in similar fashions. Isolated cells were then stained with various antibodies directed against cell surface antigens. Significant increases in both the percentages and total numbers of natural killer (NK) cells (NK1.1$^+$/CD3$^-$) and inflammatory macrophages (F4/80$^+$/Gr-1$^+$) (8, 25, 29) within the skeletal muscle tissue were detected at 5 dpi compared to those in mock-infected controls (Fig. 9A and C).
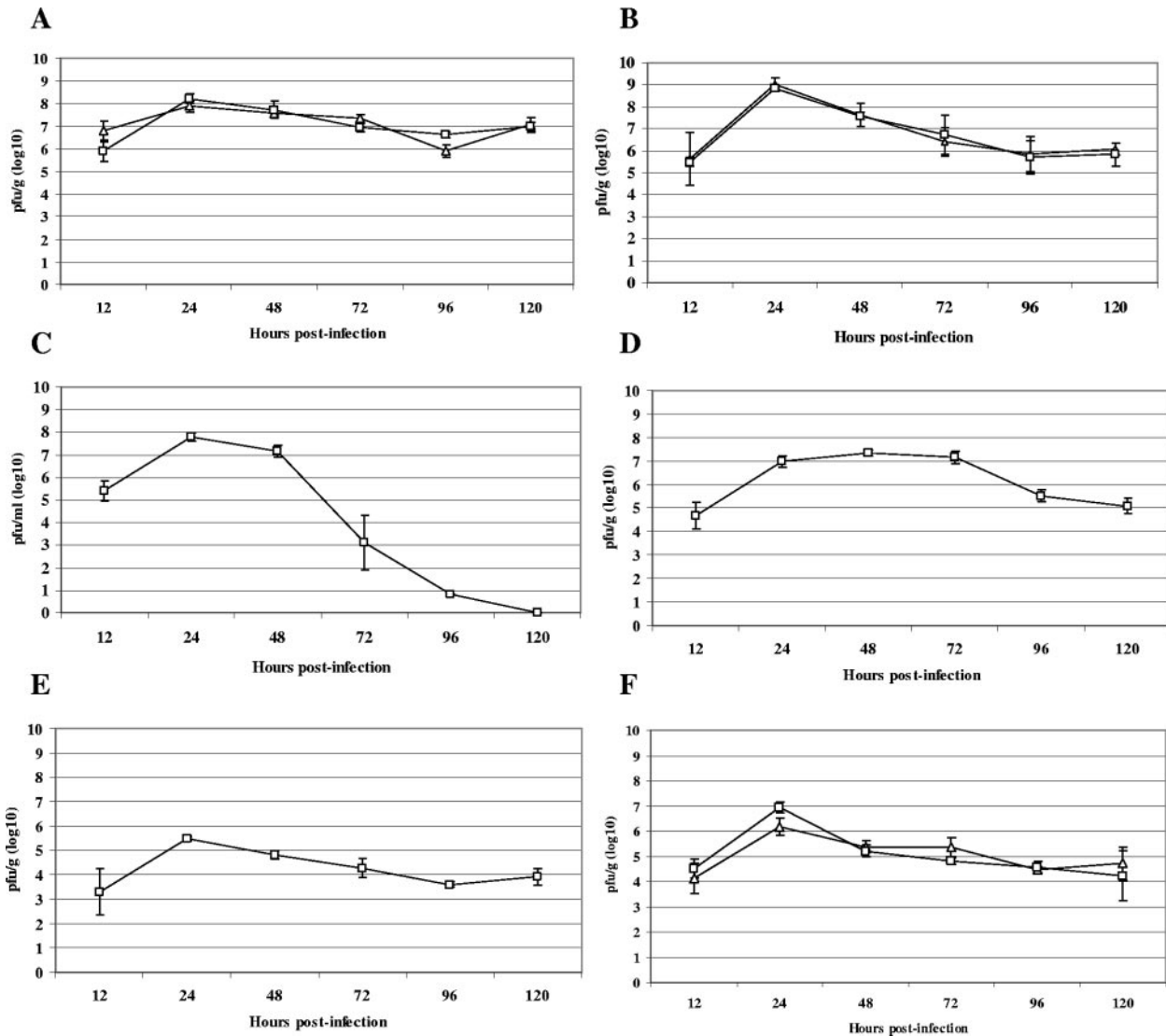
FIG. 6. Ross River virus tissue titers in 24-day-old C57BL/6J mice. Twenty-four-day-old C57BL/6J mice were infected with 10^3 PFU of RRV by subcutaneous injection in the left rear footpad. At 12, 24, 48, 72, 96, and 120 hpi, the following tissues were harvested and homogenized and the amount of infectious virus present was quantified by plaque assay on BHK-21 cells. (A) □, ankle of injected leg; Δ, ankle of noninjected leg. (B) □, quadriceps muscle of injected leg; Δ, quadriceps muscle of noninjected leg. (C) Serum. (D) Spleen. (E) Brain. (F) □, lower spinal cord; Δ, upper spinal cord. Each data point represents the arithmetic mean ± SD for three mice.

Further analyses demonstrated that the $F4/80^+/Gr-1^+$ population was also $CD11b^+/CD11c^-/B220^-$, confirming that these cells are inflammatory macrophages (data not shown). Increased numbers of both $CD4^+$ ($CD3^+$ $CD4^+$) and $CD8^+$ ($CD3^+$ $CD8^+$) T lymphocytes were also detected by 5 dpi, albeit to a much lesser extent than with both NK cells and inflammatory macrophages (Fig. 9A and C). By 7 dpi, the number of NK cells and inflammatory macrophages detected was similar to that observed at 5 dpi; however, a further increase in the total number of both $CD4^+$ and $CD8^+$ T lymphocytes was detected within the skeletal muscle tissues of infected mice (Fig. 9B and C). No significant CD19 staining was detected at 7 dpi, suggesting a lack of B lymphocytes (data not shown). In addition to identifying the above-mentioned cell types, our analyses indicated that additional cell types were

also present within the inflammatory infiltrate, such as dendritic cells. However, further studies will be required to identify the exact nature of these additional cell types.

RRV induces inflammation and disease in RAG-1$^{-/-}$ mice. Our analysis of the inflammatory infiltrates detected cells of both the innate, such as NK cells and macrophages, and adaptive, such as $CD4^+$ and $CD8^+$ T lymphocytes, arms of the immune response. However, previous studies have suggested that the RRV-induced inflammatory disease is independent of the adaptive immune response (22, 31). Therefore, to definitively determine the contribution of the adaptive immune system in the development of RRV-induced disease, 24-day-old C57BL/6J RAG-1$^{-/-}$ mice, which lack functional T and B lymphocytes (24, 33), were inoculated with 10^3 PFU of RRV in the left rear footpad and monitored for virus-induced disease.
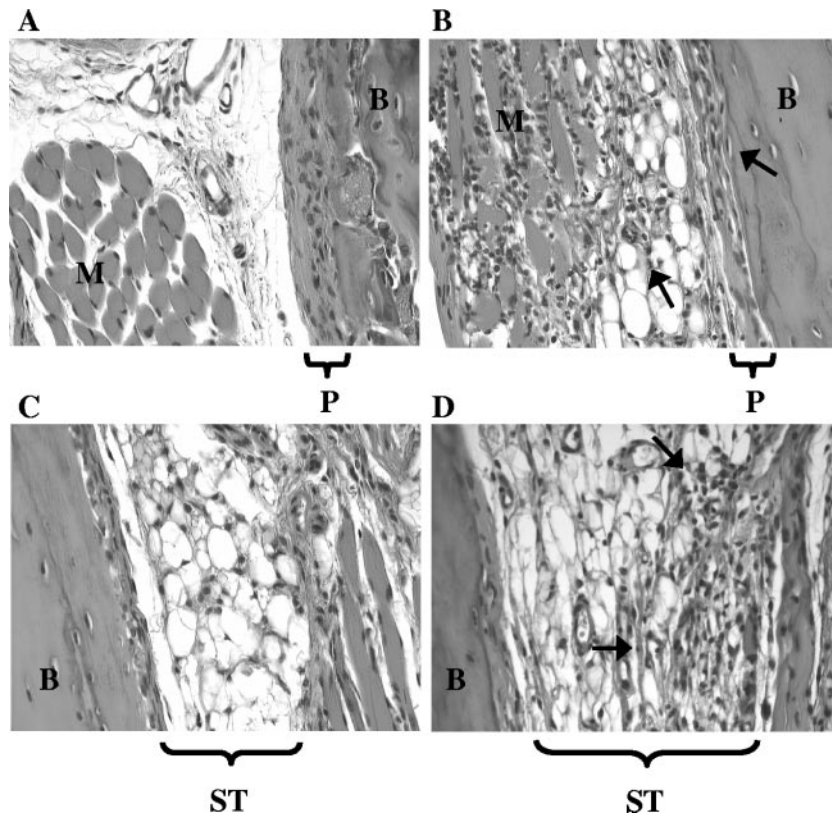
FIG. 7. Ross River virus induces inflammation in hind limb bone and joint tissues of C57BL/6J mice. Twenty-four-day-old C57BL/6J mice were infected with 10^3 PFU of RRV by subcutaneous injection in the left rear footpad. Mock-infected mice were injected with diluent alone. M, muscle; B, bone; P, periosteum; ST, synovial tissue. At 5 days (A and B) and 7 days (C and D) postinfection, mice were perfused with 4% paraformaldehyde. Following decalcification, 5-μm-thick paraffin-embedded sections generated from ankle and foot tissues of mock-infected (A and C) and RRV-infected (B and D) mice were H & E stained. Images (magnification, ×200) are representative of at least six mice per group.
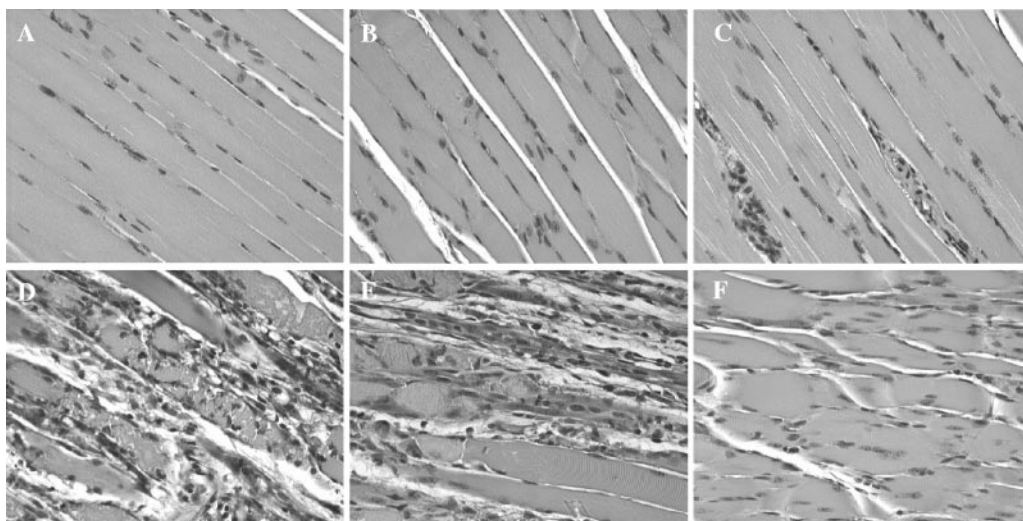

FIG. 8. Ross River virus induces inflammation in hind limb skeletal muscle tissue of C57BL/6J mice. Twenty-four-day-old C57BL/6J mice were infected with 10^3 PFU of RRV by subcutaneous injection in the left rear footpad. Mock-infected mice were injected with diluent alone. At 3, 5, 7, 10, and 30 dpi, mice were perfused with 4% paraformaldehyde and 5-μm-thick paraffin-embedded sections generated from the quadriceps muscle were H & E stained. (A) Mock infection. (B) RRV infection at 3 dpi. (C) RRV infection at 5 dpi. (D) RRV infection at 7 dpi. (E) RRV infection at 10 dpi. (F) RRV infection at 30 dpi. Images (magnification, ×200) are representative of three to six mice per group.
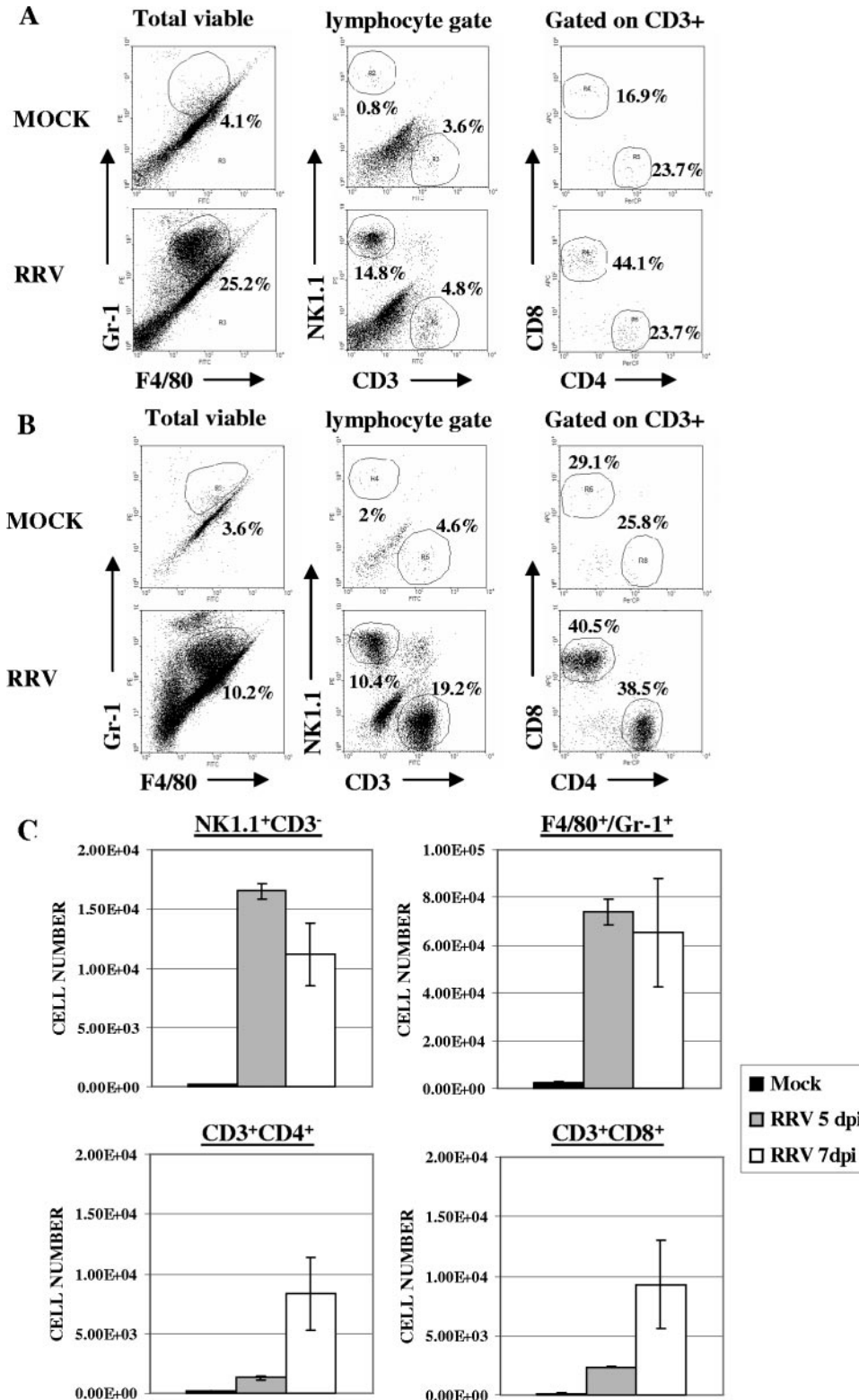
FIG. 9. Characterization of Ross River virus-induced inflammatory infiltrates. Twenty-four-day-old C57BL/6J mice were infected with 10^3 PFU of RRV by subcutaneous injection in the left rear footpad. Mock-infected mice were injected with diluent alone. (A) Cell surface staining of cells isolated from the quadriceps muscle at 5 dpi. Dot plots shown for each stain are representative of three mice. Two independent experiments gave similar results. (B) Cell surface staining of cells isolated from the quadriceps muscle at 7 dpi. Dot plots shown for each stain are representative of three mice per group. Three independent experiments gave similar results. (C) Total numbers of natural killer cells (NK1.1^{+}/CD3^{+}), inflammatory macrophages (F4/80^{+}/Gr-1^{+}), CD4 T lymphocytes (CD3^{+}/CD4^{+}), and CD8 T lymphocytes (CD3^{+}/CD8^{+}) from the quadriceps muscle of mock- and RRV-infected animals at 5 and 7 days postinfection. Data presented are the means ± standard errors of the means for three to four mice per group and are representative of at least two independent experiments.
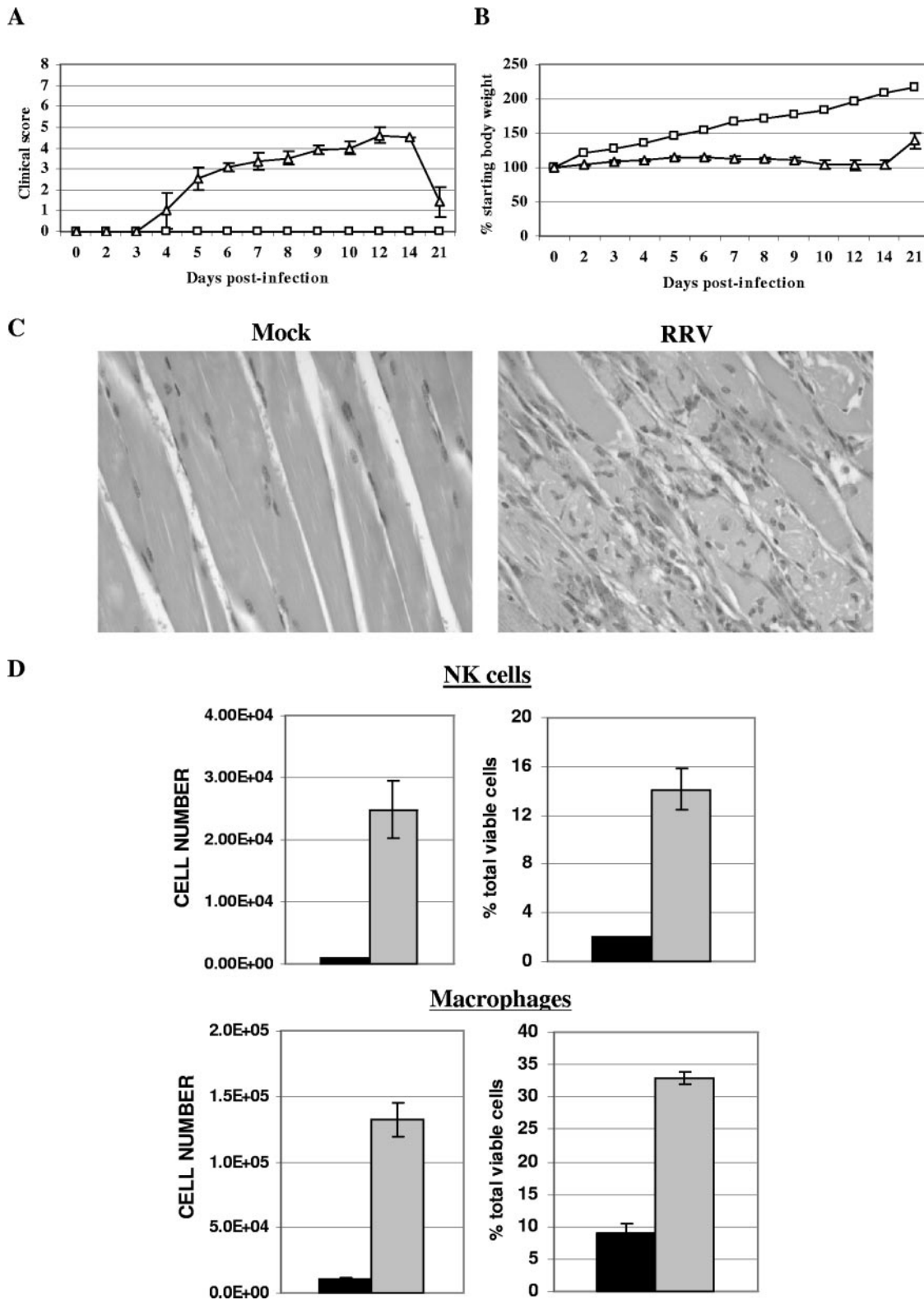
A

B

C

Mock RRV

D

NK cells

Macrophages

FIG. 10. Ross River virus-induced inflammation and disease in RAG-1$^{-/-}$. Twenty-four-day-old C57BL/6J RAG-1$^{-/-}$ mice were infected with 10^3 PFU of RRV (Δ) by subcutaneous injection in the left rear footpad. Mock-infected mice ($\square$) were injected with diluent alone. (A) Mice were scored for development of hind limb dysfunction and disease based on the following scale: 0, no disease signs; 1, ruffled fur; 2, very mild hind limb weakness; 3, mild hind limb weakness; 4, moderate hind limb weakness and dragging of hind limbs; 5, severe hind limb weakness/dragging; 6, complete loss of hind limb function; 7, moribund; and 8, death. Each data point represents the arithmetic mean ± SD for two (mock-infected) or six (RRV-infected) mice and are representative of two independent experiments. (B) Mice were monitored for weight gain or loss at 24-h intervals. Each data point represents the arithmetic mean ± SD for four (mock-infected) or six (RRV-infected) mice and are representative of two

RAG-1$^{-/-}$ mice developed disease signs similar to those observed in B6 mice, including failure to gain weight (Fig. 10B) and severe symmetrical hind limb dysfunction (Fig. 10A). The average clinical score at the peak of observable disease (day 12) in RAG-1$^{-/-}$ mice was 4.5 ± 0.38, compared to 5.9 ± 0.25 for wild-type B6 mice. Interestingly, RAG-1$^{-/-}$ mice recovered from RRV-induced disease with kinetics similar to that observed in wild-type B6 mice (Fig. 5 and 10A and B). In addition, both μMT and μMT mice depleted of T lymphocytes with anti-CD3 antibody also developed disease similar to that of wild-type mice following RRV infection (data not shown). Histological analyses demonstrated severe inflammation in the hind limb skeletal muscle (Fig. 10C) and joint-associated tissues (data not shown) of RAG-1$^{-/-}$ mice, which peaked in severity from 7 to 10 dpi. The degree of inflammation and severity of tissue destruction appeared very similar to that observed in wild-type B6 mice. We next analyzed the composition of the inflammatory infiltrates in the skeletal muscle by flow cytometry. Similar to what was observed in wild-type B6 mice, increases in the percentage and total number of inflammatory macrophages (F4/80$^+$/Gr-1$^+$) and NK cells (NK1.1$^+$/CD3$^-$) in the quadriceps muscle of RRV-infected RAG-1$^{-/-}$ mice compared to those in mock-infected controls were detected (Fig. 10E). CD3$^+$ T lymphocytes were not detected within the skeletal muscle tissues or spleens of RAG-1$^{-/-}$ mice, confirming the lack of T lymphocytes in these mice (data not shown). As was observed for the wild-type B6 mice, there were additional cell populations present, including dendritic cells (data not shown), that will require additional analysis to fully characterize.

DISCUSSION

The pathogenesis of alphavirus-induced arthritides, which represent a significant worldwide disease threat, is poorly understood. Therefore, the recently described mouse model of RRV-induced inflammation was used to study viral tropism and the composition of the virus-induced inflammatory response. This report extends earlier work with the RRV mouse model by demonstrating that the primary targets of Ross River virus infection in outbred CD-1 mice and inbred adult B6 mice are bone, joint, and skeletal muscle tissues. Significantly, further analyses demonstrated that RRV infection of adult B6 mice resulted in severe inflammation within these same tissues. In addition to inflammatory macrophages and NK cells, CD4$^+$ and CD8$^+$ T lymphocytes were found to be major components of the virus-induced inflammatory response. However, RAG-1$^{-/-}$ mice developed disease signs and infiltration of NK cells and macrophages similar to those of wild-type B6 mice, suggesting that the adaptive immune response does not play a critical role in the development of disease. These studies demonstrate that the mouse model of RRV disease will greatly facilitate the identification of viral and host factors which contribute to the induction and resolution of this severe inflammatory disease.

The detection of RRV in multiple bone and joint-associated tissues, such as synovial tissue, periosteum, tendons, and ligaments, has not previously been described. These findings are consistent with observations of RRV-infected humans in whom both viral antigen and viral RNA have been detected from synovial effusions and synovial biopsy samples (6). Additionally, infectious virus was detectable in the ankle joints of RRV-infected mice by plaque assay by 12 hpi; however, infectious RRV has not yet been recovered from the joints of RRV-infected patients (13). Similar to previous reports, high titers of RRV were also detected within skeletal muscle tissues of infected mice (22, 26, 31). However, our targeting studies demonstrated that there were very few RRV-infected muscle fibers in the hind limbs at early times postinfection. By 48 to 72 hpi, large areas of RRV-infected muscle fibers were observed in hind limb skeletal muscle tissue. These findings raise the possibility that RRV may initially infect joint- or skeletal muscle-associated connective tissues and subsequently spread into skeletal muscle myofibers. Direct infection of skeletal muscle tissue by RRV in humans has not been demonstrated, although 60% of patients diagnosed with Ross River virus disease experience myalgia (12). The route and spread of RRV from the initial site of infection to joint and skeletal muscle tissue have not been characterized fully. Studies performed with other alphaviruses, such as Venezuelan equine encephalitis virus, have suggested that this group of viruses may initially infect skin dendritic cells (23). The infected dendritic cells migrate to the draining lymph node, where the virus undergoes additional rounds of replication and seeds a high-titer serum viremia, resulting in viral spread to target tissues.

Histological analyses of tissues from adult B6 mice revealed that RRV infection induced inflammation within joint-associated tissues, such as periosteum, tendons, and synovial tissue, as well as skeletal muscle tissue. Inflammatory infiltrates were first observed within these hind limb tissues at 5 dpi, peaked at 7 to 10 dpi, and were dramatically decreased in number by 20 to 30 dpi. The occurrence of inflammation within these tissues occurred well after peak viral titers and correlated with the observed hind limb weakness, which was first detectable at 4 to 5 dpi, became increasingly severe from 7 to 12 dpi, and resolved between 20 to 30 dpi. Although RRV has been reported to induce encephalomyelitis characterized by central nervous system demyelination in 1-week-old BALB/c mice (32), we found no evidence of virus-induced inflammation, demyelination, or other pathology in the brains or spinal cords of 24-day-old adult B6 mice. RRV infection of 7-day-old BALB/c mice was also proposed to cause muscle destruction in the absence of a host immune response (31), while immune pathology clearly contributes to virus-induced pathology in our system. The differences in mouse age and strain used in the two

independent experiments. (C) At 10 days postinfection, mice were perfused with 4% paraformaldehyde and 5-μm-thick paraffin-embedded sections generated from the quadriceps muscle were H & E stained. Images (magnification, ×200) are representative of three mice per group. (D) Total numbers and percentages of natural killer cells (NK1.1$^+$/CD3$^-$) and inflammatory macrophages (F4/80$^+$/Gr-1$^+$) from the quadriceps muscles of mock-infected (black bars) or RRV-infected (gray bars) RAG-1$^{-/-}$ mice at 7 days postinfection. Data presented are the means ± standard errors of the means for three mice per group and are representative of two independent experiments.

studies may explain the differences between our results and those previously reported. In addition, it has also been reported that, in contrast to 1-week-old BALB/c mice, 4-week-old BALB/c mice infected with RRV developed little to no disease signs (31), indicating there are age- and strain-dependent effects of RRV infection. Taken together, our findings suggest that the observed disease signs in 24-day-old B6 mice are most likely due to virus-induced pathology in hind limb tissues.

Consistent with previous work, our studies identified inflammatory macrophages as major constituents of the inflammatory infiltrate in hind limb skeletal muscles of RRV-infected mice. The presence of inflammatory macrophages, as well as a large increase of NK cells, was readily detectable by 5 dpi. By 7 dpi, increased numbers of both $CD4^+$ and $CD8^+$ T lymphocytes were also found within hind limb skeletal muscle tissue. Although our studies focused on the skeletal muscle, the cellular composition of inflammation identified is similar to what has been reported following RRV infection of humans. Both NK cells and macrophages have been detected within synovial exudates from the knees of RRV-infected patients (6, 14, 35). In addition, $CD4^+$ and $CD8^+$ T lymphocytes were detected in synovial tissue sections generated from knee joint biopsies (35).

A recent study demonstrated that treatment of mice with macrophage-toxic agents prior to infection completely prevented RRV-induced muscle inflammation (22), suggesting an important role for innate immune responses in the development of RRV-induced disease. Our studies of RAG-$1^{-/-}$ mice, which develop inflammation and disease similar to those of wild-type B6, underscore the importance of the innate immune response. However, we cannot rule out the possibility of a limited contribution of the adaptive response to the severity of disease. In addition, RAG-$1^{-/-}$ mice recovered from RRV-induced disease with kinetics similar to that observed in wild-type B6 mice. Future studies will be aimed at determining whether innate immune mechanisms are sufficient to control RRV infection or whether other mechanisms are involved in the resolution of disease in RAG-$1^{-/-}$ mice.

Infection of neonatal mice with the Tucson strain of coxsackievirus B1 ($CVB1_T$) or 10- to 14-day-old mice with the DA strain of Theiler's murine encephalomyelitis virus has also been shown to induce severe myositis in hind limb skeletal muscle tissue (9, 28). Whereas the role of the immune response in Theiler's murine encephalomyelitis virus-induced disease is not well understood, T lymphocytes have been demonstrated to play a major role in $CVB1_T$-induced disease (41), suggesting that RRV and $CVB1_T$ may promote muscle pathology by distinct mechanisms.

The mechanisms by which RRV or other arthritogenic alphaviruses trigger inflammatory responses are not understood. Interestingly, when injected directly into murine knee joints, double-stranded RNA (dsRNA) (which is formed during the replication and transcription of RNA viruses such as RRV) is itself arthritogenic (42). In addition, similarly to the critical role of macrophages in the development of RRV-induced disease, depletion of monocytes completely prevented dsRNA-induced arthritis. T and B lymphocytes were also found to be dispensable for the development of dsRNA-induced arthritis (42). A number of different molecules have been demonstrated to contribute to the host's detection of viral dsRNA. Toll-like receptor 3 was not required for dsRNA-induced arthritis (42); therefore, it will be interesting to determine the role of other sensors of dsRNA in the development of RRV-induced disease, such as protein kinase R (4), or the newly identified caspase activation and recruitment domain-containing RNA helicases retinoic acid-inducible gene I (40) and mda-5 (1).

In addition to RRV, Chikungunya virus, O'nyong-nyong virus, and Mayaro virus, Sindbis group alphaviruses are also associated with arthritis and arthralgia in humans (10). However, studies of adult mice have demonstrated that infection with most Sindbis group alphaviruses results in encephalitic disease (11, 37). Recent work has demonstrated that Sindbis group alphaviruses, such as S.A.AR86 and TR339, replicated in bone and joint-associated tissues of adult CD-1 mice; however, virus-induced inflammation or other pathology was not observed within these tissues (15). Therefore, the RRV mouse model represents a unique system for studying the pathogenesis of alphavirus-induced inflammatory disease in bone, joint, and skeletal muscle tissue.

REFERENCES

1. **Andrejeva, J., K. S. Childs, D. F. Young, T. S. Carlos, N. Stock, S. Goodbourn, and R. E. Randall.** 2004. The V proteins of paramyxoviruses bind the IFN-inducible RNA helicase, mda-5, and inhibit its activation of the IFN-beta promoter. Proc. Natl. Acad. Sci. USA **101:**17264–17269.
2. **Charge, S. B., and M. A. Rudnicki.** 2004. Cellular and molecular regulation of muscle regeneration. Physiol. Rev. **84:**209–238.
3. **Dalgarno, L., C. M. Rice, and J. H. Strauss.** 1983. Ross River virus 26 s RNA: complete nucleotide sequence and deduced sequence of the encoded structural proteins. Virology **129:**170–187.
4. **Diebold, S. S., M. Montoya, H. Unger, L. Alexopoulou, P. Roy, L. E. Haswell, A. Al-Shamkhani, R. Flavell, P. Borrow, and C. Reise Sousa.** 2003. Viral infection switches non-plasmacytoid dendritic cells into high interferon producers. Nature **424:**324–328.
5. **Doherty, R. L., R. H. Whitehead, B. M. Gorman, and A. K. O'Gower.** 1963. The isolation of a third group A arbovirus in Australia, with preliminary observations on its relationship to epidemic polyarthritis. Aust. J. Sci. **26:**183–184.
6. **Fraser, J. R., A. L. Cunningham, B. J. Clarris, J. G. Aaskov, and R. Leach.** 1981. Cytology of synovial effusions in epidemic polyarthritis. Aust. N. Z. J. Med. **11:**168–173.
7. **Fraser, J. R., V. M. Ratnamohan, J. P. Dowling, G. J. Becker, and G. A. Varigos.** 1983. The exanthem of Ross River virus infection: histology, location of virus antigen and nature of inflammatory infiltrate. J. Clin. Pathol. **36:**1256–1263.
8. **Geissmann, F., S. Jung, and D. R. Littman.** 2003. Blood monocytes consist of two principal subsets with distinct migratory properties. Immunity **19:**71–82.
9. **Gomez, R. M., J. E. Rinehart, R. Wollmann, and R. P. Roos.** 1996. Theiler's murine encephalomyelitis virus-induced cardiac and skeletal muscle disease. J. Virol. **70:**8926–8933.
10. **Griffin, D. E.** 2001. Alphaviruses, p. 917–962. In P. M. Howley, P. M. Howley, et al. (ed.), Fields virology, 4th ed. Lippincott, Williams, & Wilkins, Philadelphia, Pa.
11. **Griffin, D. E., and R. T. Johnson.** 1977. Role of the immune response in recovery from Sindbis virus encephalitis in mice. J. Immunol. **118:**1070–1075.
12. **Harley, D., D. Bossingham, D. M. Purdie, N. Pandeya, and A. C. Sleigh.** 2002. Ross River virus disease in tropical Queensland: evolution of rheumatic manifestations in an inception cohort followed for six months. Med. J. Aust. **177:**352–355.

13. **Harley, D., A. Sleigh, and S. Ritchie.** 2001. Ross River virus transmission, infection, and disease: a cross-disciplinary review. Clin. Microbiol. Rev. **14:** 909–932.
14. **Hazelton, R. A., C. Hughes, and J. G. Aaskov.** 1985. The inflammatory response in the synovium of a patient with Ross River arbovirus infection. Aust. N. Z. J. Med. **15:**336–339.
15. **Heise, M. T., D. A. Simpson, and R. E. Johnston.** 2000. Sindbis-group alphavirus replication in periosteum and endosteum of long bones in adult mice. J. Virol. **74:**9294–9299.
16. **Heise, M. T., L. J. White, D. A. Simpson, C. Leonard, K. A. Bernard, R. B. Meeker, and R. E. Johnston.** 2003. An attenuating mutation in nsP1 of the Sindbis-group virus S.A.AR86 accelerates nonstructural protein processing and up-regulates viral 26S RNA synthesis. J. Virol. **77:**1149–1156.
17. **Kitamura, D., J. Roes, R. Kuhn, and K. Rajewsky.** 1991. A B cell-deficient mouse by targeted disruption of the membrane exon of the immunoglobulin mu chain gene. Nature **350:**423–426.
18. **Kiwanuka, N., E. J. Sanders, E. B. Rwaguma, J. Kawamata, F. P. Ssengooba, R. Najjemba, W. A. Were, M. Lamunu, G. Bagambisa, T. R. Burkot, L. Dunster, J. J. Lutwama, D. A. Martin, C. B. Cropp, N. Karabatsos, R. S. Lanciotti, T. F. Tsai, and G. L. Campbell.** 1999. O'nyong-nyong fever in south-central Uganda, 1996–1997: clinical features and validation of a clinical case definition for surveillance purposes. Clin. Infect. Dis. **29:**1243–1250.
19. **Klapsing, P., J. D. MacLean, S. Glaze, K. L. McClean, M. A. Drebot, R. S. Lanciotti, and G. L. Campbell.** 2005. Ross River virus disease reemergence, Fiji, 2003–2004. Emerg. Infect. Dis. **11:**613–615.
20. **Kuhn, R. J., H. G. Niesters, Z. Hong, and J. H. Strauss.** 1991. Infectious RNA transcripts from Ross River virus cDNA clones and the construction and characterization of defined chimeras with Sindbis virus. Virology **182:** 430–441.
21. **Laras, K., N. C. Sukri, R. P. Larasati, M. J. Bangs, R. Kosim, Djauzi, T. Wandra, J. Master, H. Kosasih, S. Hartati, C. Beckett, E. R. Sedyaningsih, H. J. Beecham III, and A. L. Corwin.** 2005. Tracking the re-emergence of epidemic chikungunya virus in Indonesia. Trans. R. Soc. Trop. Med. Hyg. **99:**128–141.
22. **Lidbury, B. A., C. Simeonovic, G. E. Maxwell, I. D. Marshall, and A. J. Hapel.** 2000. Macrophage-induced muscle pathology results in morbidity and mortality for Ross River virus-infected mice. J. Infect. Dis. **181:**27–34.
23. **MacDonald, G. H., and R. E. Johnston.** 2000. Role of dendritic cell targeting in Venezuelan equine encephalitis virus pathogenesis. J. Virol. **74:**914–922.
24. **Mombaerts, P., J. Iacomini, R. S. Johnson, K. Herrup, S. Tonegawa, and V. E. Papaioannou.** 1992. RAG-1-deficient mice have no mature B and T lymphocytes. Cell **68:**869–877.
25. **Mordue, D. G., and L. D. Sibley.** 2003. A novel population of Gr-1$^+$-activated macrophages induced during acute toxoplasmosis. J. Leukoc. Biol. **74:**1015–1025.
26. **Murphy, F. A., W. P. Taylor, C. A. Mims, and I. D. Marshall.** 1973. Pathogenesis of Ross River virus infection in mice. II. Muscle, heart, and brown fat lesions. J. Infect. Dis. **127:**129–138.
27. **Pastorino, B., J. J. Muyembe-Tamfum, M. Bessaud, F. Tock, H. Tolou, J. P. Durand, and C. N. Peyrefitte.** 2004. Epidemic resurgence of Chikungunya virus in democratic Republic of the Congo: identification of a new central African strain. J. Med. Virol. **74:**277–282.
28. **Ray, C. G., L. L. Minnich, and P. C. Johnson.** 1979. Selective polymyositis inducted by coxsackievirus B1 in mice. J. Infect. Dis. **140:**239–243.
29. **Robben, P. M., M. Laregina, W. A. Kuziel, and L. D. Sibley.** 2005. Recruitment of Gr-1+ monocytes is essential for control of acute toxoplasmosis. J. Exp. Med. **201:**1761–1769.
30. **Rwaguma, E. B., J. J. Lutwama, S. D. Sempala, N. Kiwanuka, J. Kamugisha, S. Okware, G. Bagambisa, R. Lanciotti, J. T. Roehrig, and D. J. Gubler.** 1997. Emergence of epidemic O'nyong-nyong fever in southwestern Uganda, after an absence of 35 years. Emerg. Infect. Dis. **3:**77.
31. **Seay, A. R., D. E. Griffin, and R. T. Johnson.** 1981. Experimental viral polymyositis: age dependency and immune responses to Ross River virus infection in mice. Neurology **31:**656–660.
32. **Seay, A. R., and J. S. Wolinsky.** 1982. Ross River virus-induced demyelination: I. Pathogenesis and histopathology. Ann. Neurol. **12:**380–389.
33. **Shinkai, Y., G. Rathbun, K. P. Lam, E. M. Oltz, V. Stewart, M. Mendelsohn, J. Charron, M. Datta, F. Young, A. M. Stall, et al.** 1992. RAG-2-deficient mice lack mature lymphocytes owing to inability to initiate V(D)J. rearrangement. Cell **68:**855–867.
34. **Simpson, D. A., N. L. Davis, S. C. Lin, D. Russell, and R. E. Johnston.** 1996. Complete nucleotide sequence and full-length cDNA clone of S.A.AR86 a South African alphavirus related to Sindbis. Virology **222:**464–469.
35. **Soden, M., H. Vasudevan, B. Roberts, R. Coelen, G. Hamlin, S. Vasudevan, and J. La Brooy.** 2000. Detection of viral ribonucleic acid and histologic analysis of inflamed synovium in Ross River virus infection. Arthritis Rheum. **43:**365–369.
36. **Suhrbier, A., and M. La Linn.** 2004. Clinical and pathologic aspects of arthritis due to Ross River virus and other alphaviruses. Curr. Opin. Rheumatol. **16:**374–379.
37. **Suthar, M. S., R. Shabman, K. Madric, C. Lambeth, and M. T. Heise.** 2005. Identification of adult mouse neurovirulence determinants of the Sindbis virus strain AR86. J. Virol. **79:**4219–4228.
38. **Tidball, J. G.** 2005. Inflammatory processes in muscle injury and repair. Am. J. Physiol. Regul. Integr. Comp. Physiol. **288:**R345–R353.
39. **Williams, M. C., J. P. Woodall, and J. D. Gillett.** 1965. O'nyong-Nyong fever: an epidemic virus disease in East Africa. VII. Virus isolations from man and serological studies up to July 1961. Trans. R. Soc. Trop. Med. Hyg. **59:**186–197.
40. **Yoneyama, M., M. Kikuchi, T. Natsukawa, N. Shinobu, T. Imaizumi, M. Miyagishi, K. Taira, S. Akira, and T. Fujita.** 2004. The RNA helicase RIG-I has an essential function in double-stranded RNA-induced innate antiviral responses. Nat. Immunol. **5:**730–737.
41. **Ytterberg, S. R., M. L. Mahowald, and R. P. Messner.** 1987. Coxsackievirus B 1-induced polymyositis. Lack of disease expression in nu/nu mice. J. Clin. Investig. **80:**499–506.
42. **Zare, F., M. Bokarewa, N. Nenonen, T. Bergstrom, L. Alexopoulou, R. A. Flavell, and A. Tarkowski.** 2004. Arthritogenic properties of double-stranded (viral) RNA. J. Immunol. **172:**5656–5663.